CHAPTER 4

Chemical Vapor Texturing Process of ZnO Photoelectrodes

A chemical vapor texturing process is introduced to solve some uncontrollable factors of the chemical wet texturing process such as a random in texturing direction, decrease in texturing rate and substrate damage [73]. The vapor texturing process is an interesting technique for better surface modification due to its more advantage than the wet texturing process [74-76]. In addition, it has an achievement in an effective low cost and simplicity. The vapor texturing process is a widely used for modifying surface of silicon wafer. An achievement in external quantum efficiency (EQE) is demonstrated by a vapor texturing process of acid solution [75]. A better uniform and homogeneous surface morphology of silicon wafer is observed after the vapor texturing process. A reflectance shows a significant reduction in comparison to a conventional wet texturing process. These results lead an enhancement in PCE for silicon solar cell application which is dominant correlation to increase in J_{sc}. Moreover, a metal assisted for a vapor texturing process shows a very low reflectivity nearly to 2% due to porous layer formation [74]. The porous film affects an efficient light trapping. A sequential texturing process of multicrystalline silicon (mc-Si) using a saw damage removal with texturing (SDRWT) and vapor texturing shows an improvement in surface morphology and decrease in reflectance [54]. For solar cell application, the decreasing reflectance shows an effectively relate to an improvement in J_{sc} and PCE. Moreover, the process demonstrates ability for an industrial scale production. Nevertheless, a development in a ZnO:Al (AZO) film is reported [77]. The AZO film shows a successfully modified using a vapor texturing process using HF solution and results an improvement in a diffused transmittance.

In this chapter, an acid vapor texturing process is used to modify ZnO films for DSSCs application. Morphology, dye adsorption, light scattering, and DSSCs performance are discussed.

4.1 Chemical vapor texturing process

An acid solution of HNO_3 (65% AR., RCI Labscan) was used for the vapor texturing process. The solution (20 mL) was prepared in a texturing bath and a ZnO film was placed over the bath and maintained for texturing time of 2, 4, 6 and 8 min as can be seen in the figure 4.1. After the texturing process, the film was rinsed and annealed. To maintain a texturing rate, a stirring bar is used for continuously evaporating the solution from liquid phase to vapor phase. Moreover, a texturing surface can be targeted in the vertical direction of the flowing vapor.

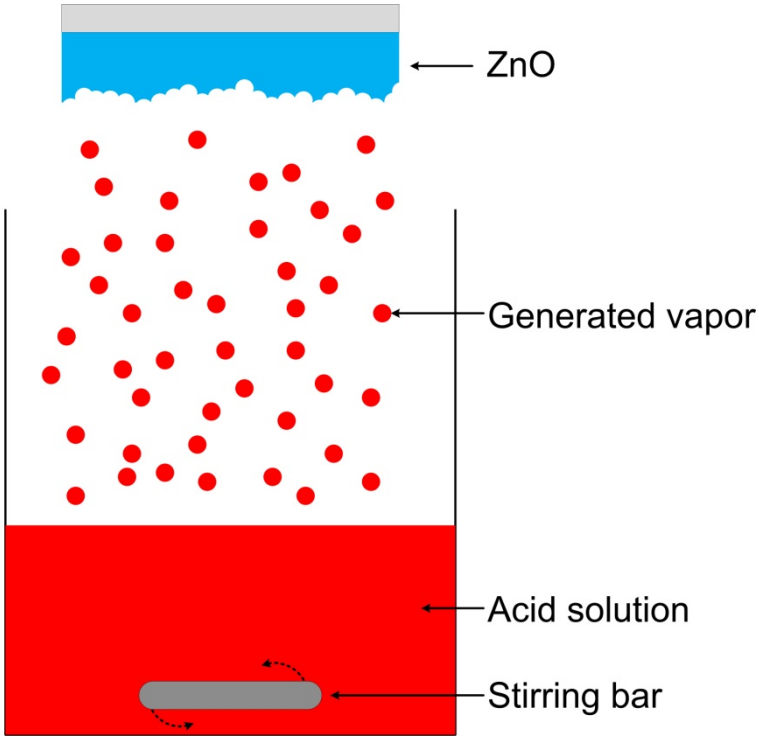

Figure 4.1 Schematic diagram of an experimental set up for vapor texturing process. Reproduced with permission from ref [78]. Copyright (2016) Elsevier.

4.2 Morphology

Figure 4.2 shows top view FE-SEM images of the ZnO films texturing at various texturing times. After the texturing process, changes in surface morphology include roughness and pore formation is clearly observed. The texturing films show smoother surface than the non-texturing films consistent with a formation of small pores. For the short texturing time of 2 - 4 min, small pore formation is found. The pore becomes larger size for the long texturing time (6 min). Moreover, it deforms until to disappear (8 min). The formation of small pores can be described by aggregate particles at the surface are removed during the beginning of the texturing process. On the other hand, both of the aggregate particles and deeper layer particles are removed by a continuous chemical reaction due to an over texturing for a longer texturing time. The chemical reaction between HNO_3 vapor and ZnO during the texturing process to remove particles can be described as following reaction [60],

$$2HNO_3 + ZnO \rightarrow Zn(NO_3)_2 + H_2O \quad (4.1)$$

After the HNO_3 solution is evaporated to form a vapor phase and attacked the films, the ZnO will be dissolute to form $Zn(NO_3)_2$ at the surface. The reaction is continuously occurred until the rinsing step with the flowing distilled water to stop the reaction. The dissolution leads a formation of pore structure.

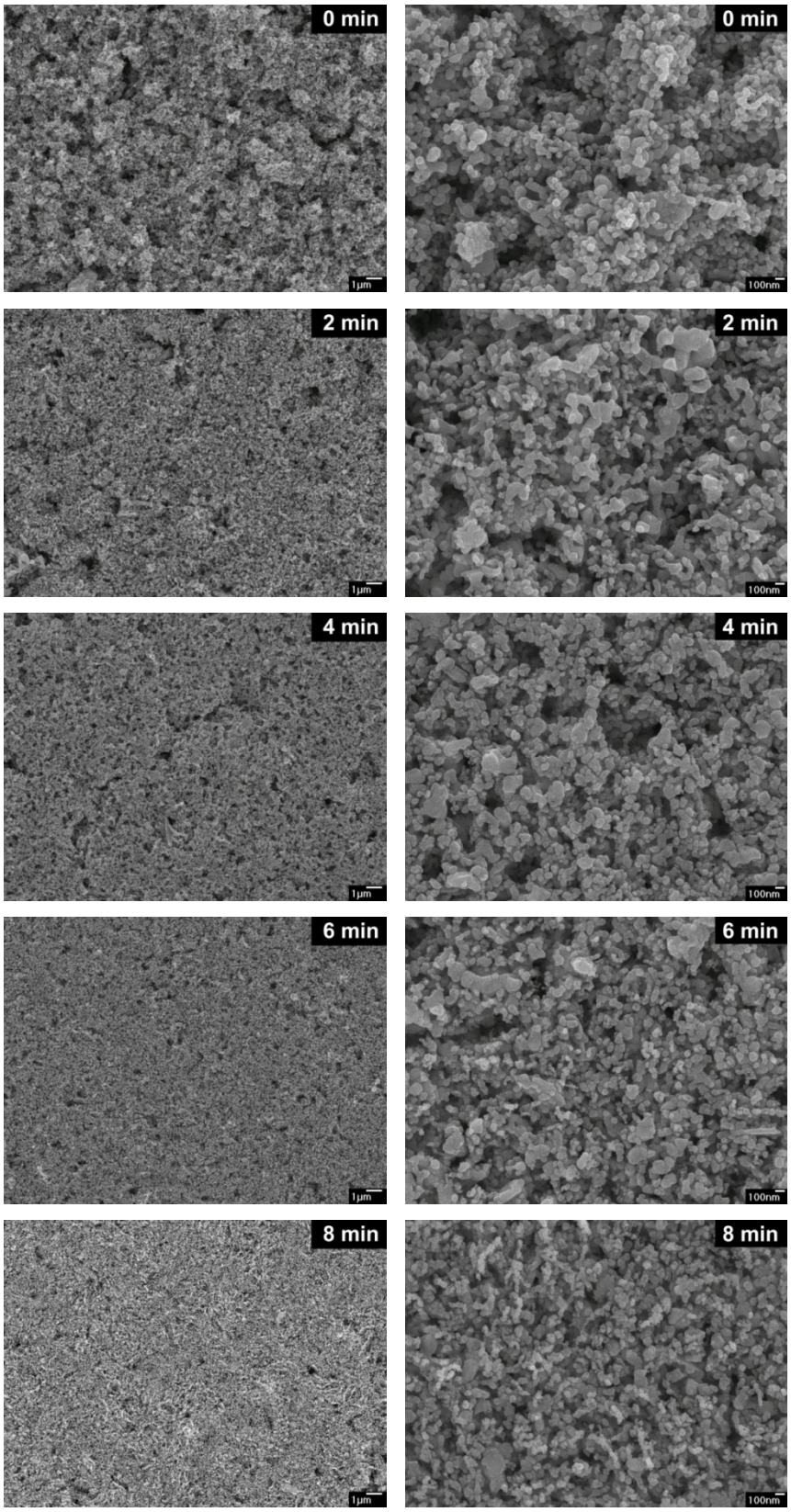

Figure 4.2 Low (left) and high (right) morphological magnification of acid vapor texturing films.

Films thickness was measured from cross-sectional FE-SEM images (figure 4.3) using image-J software and listed in table 4.1. Relationship between thickness and texturing time show a strong negative linear trend (R^2 = 0.98). A texturing rate is calculated based on these results (figure 4.4) and it is at around 1.12 μm/min.

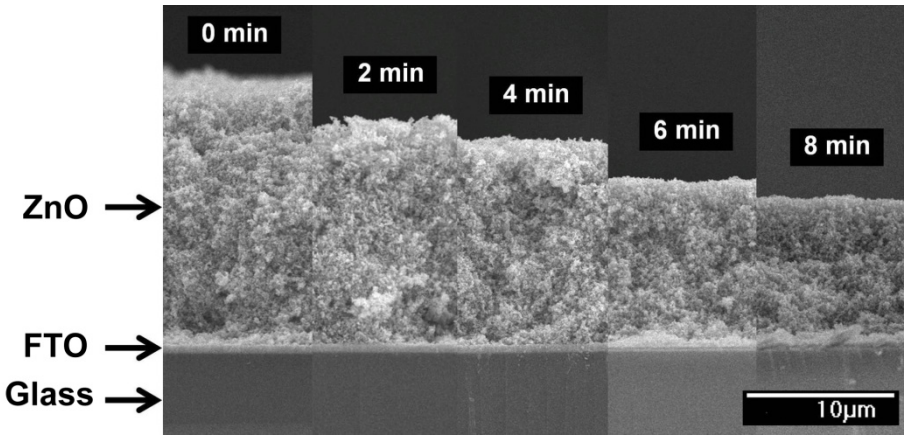

Figure 4.3 Cross-sectional images of acid vapor texturing films. Reproduced with permission from ref [78]. Copyright (2016) Elsevier.

Table 4.1 Measured thickness of acid vapor texturing films. Reproduced with permission from ref [78]. Copyright (2016) Elsevier.

Texturing time (min)	Average (μm)	SD (μm)	Max (μm)	Min (μm)
0	18.45	0.27	19.20	18.10
2	15.21	0.45	16.20	14.50
4	14.08	0.24	14.70	13.80
6	11.44	0.15	11.80	11.10
8	9.84	0.39	10.60	9.30

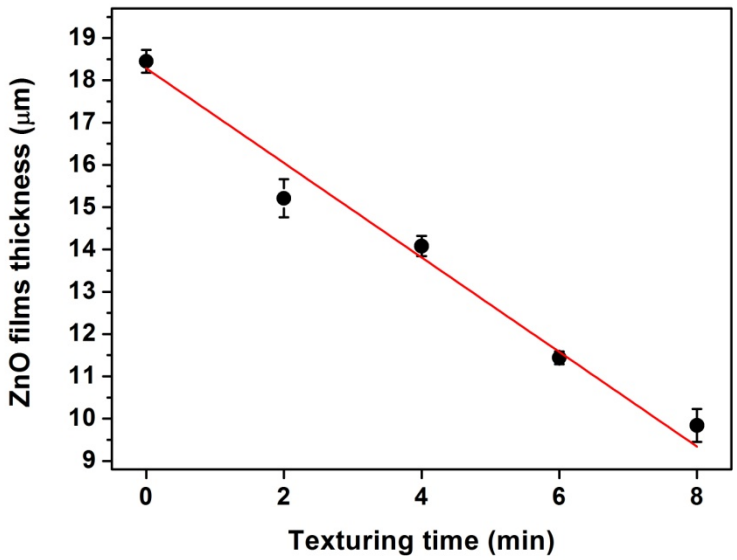

Figure 4.4 A linear fitting curve of films thickness. Reproduced with permission from ref [78]. Copyright (2016) Elsevier.

4.3 Simulated 3D profile analysis

A simulated 3D profile was simulated as shown in figure 4.5 to finely investigate the morphology. Peak (blue zone) and through (yellow zone) denote aggregate particles at the surface and pore position, respectively. A slight decrease of the peak is found after the texturing process indicating that aggregate particles at the surface is removed, this effect result a pore formation for the short texturing time. On the other hand, the texturing films for longer texturing time become a planar films as can be seen that the peak and through are slightly disappeared.

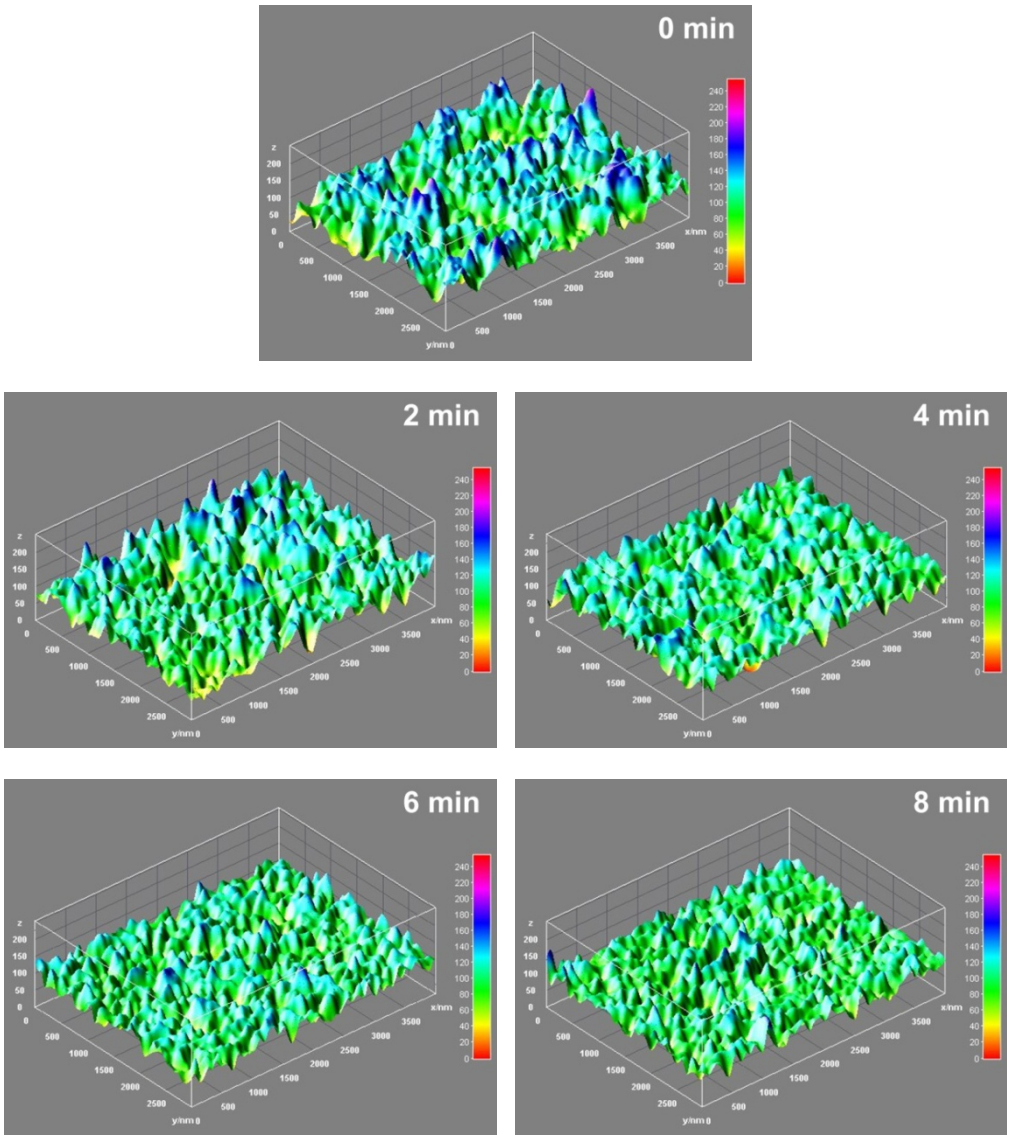

Figure 4.5 Simulated 3D profiles of acid vapor texturing films. Reproduced with permission from ref [78]. Copyright (2016) Elsevier.

The 3D profile results are consistent with a decrease in relative roughness which was calculated using the image-J software as can be seen in figure 4.6. Therefore, it can be concluded that a texturing time of 4 min might be an appropriate condition because a balancing between aggregate particles removal and pore formation.

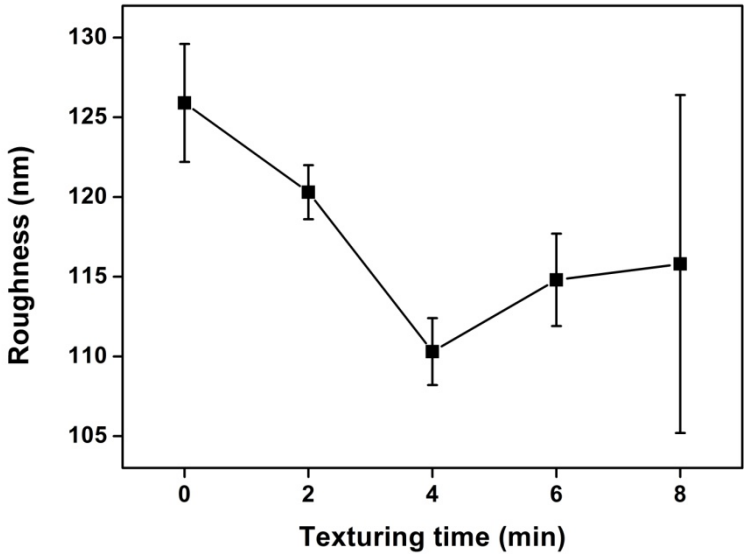

Figure 4.6 Relative roughness of acid vapor texturing films.

4.4 Pore analysis

Pore density was analyzed using image-J software to examine surface pore characterization [79]. Figure 4.7 shows a slightly increased of the pore density for the short texturing time. The maximum pore density of 11.2×10^2 pores/μm^2 is observed at the texturing time of 4 min in comparison to the non-texturing films of 8.04×10^2 pores/μm^2, and it is rapidly decreased for the longer texturing time. This result is consistent with SSAs, the measured SSAs under N_2 gas are 2.5 m^2/g and 8.2 m^2/g for the non-texturing films and the texturing films with texturing time of 4 min, respectively. From these results, it can be confirmed that pore density and SSA are in a direct correlation.

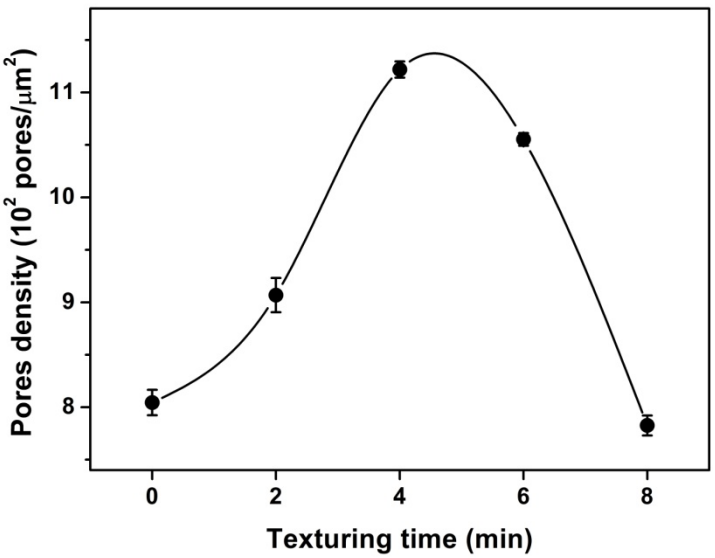

Figure 4.7 Pore density of acid vapor texturing films. Reproduced with permission from ref [78]. Copyright (2016) Elsevier.

Pore size and shape factor were investigated to better understand the pore characterization [80]. The ordinary FE-SEM image was initially converted to be a binary image (image >> type >> 8-bit). Next, verifying the pore position (image >> adjust >> threshold >> auto) and analyzing the pore size and shape factor (analyze >> analyze particles). Finally, the pore size and shape factor were counted. Pore size distribution shows a dominant count frequency in the range of 0-5 nm for all conditions as can be seen in figure 4.8. Moreover, the texturing films at short texturing time showed higher count frequency than the non-texturing film. The result implied that small porous films are formed after texturing due to the chemical reaction.

Figure 4.9 presents shape factor, the maximum count frequency is significantly observed in range of 0.8-1.0. The shape factor is defined between 0 and 1 refer to an irregular pore and circular pore, respectively. From the results, it can be interpreted that most of the pores are formed circular which is an efficient shape for supporting better dye adsorption as shown in figure 4.10. During the dye adsorption process, dye molecules have more interfacial contact with circular pores than the irregular pores. The result leads an improved dye adsorption for the circular porous films. Moreover, the better interfacial contact will lead a stronger chemical bond between the dye molecules

and films. On the other hand, the weaker bond will be happen for the irregular pores which affecting an easy removal of dye molecules due to inefficient interfacial contact.

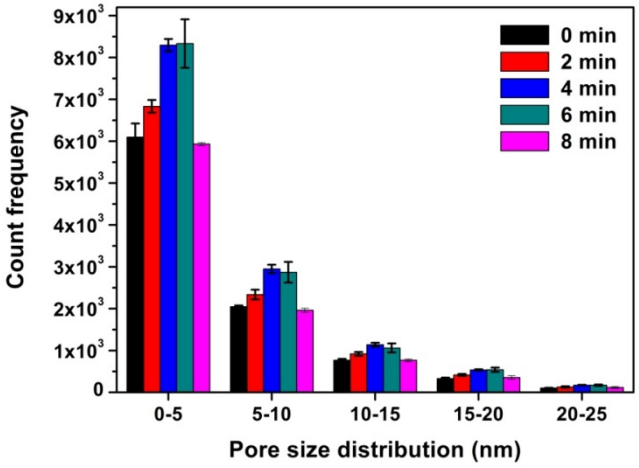

Figure 4.8 Pore size distribution of acid vapor texturing films. Reproduced with permission from ref [78]. Copyright (2016) Elsevier.

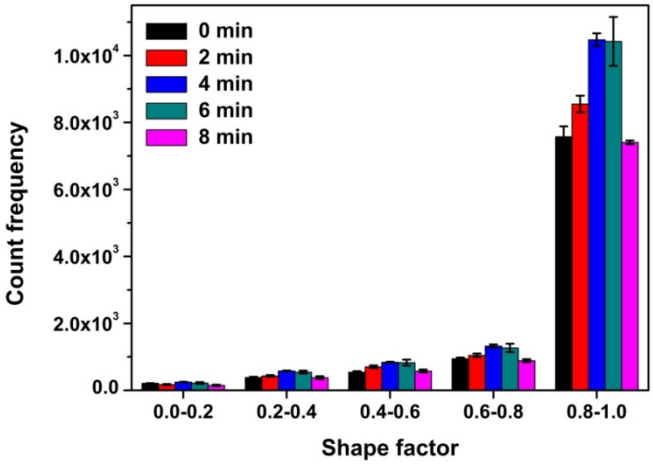

Figure 4.9 Pore shape factor of acid vapor texturing films. Reproduced with permission from ref [78]. Copyright (2016) Elsevier.

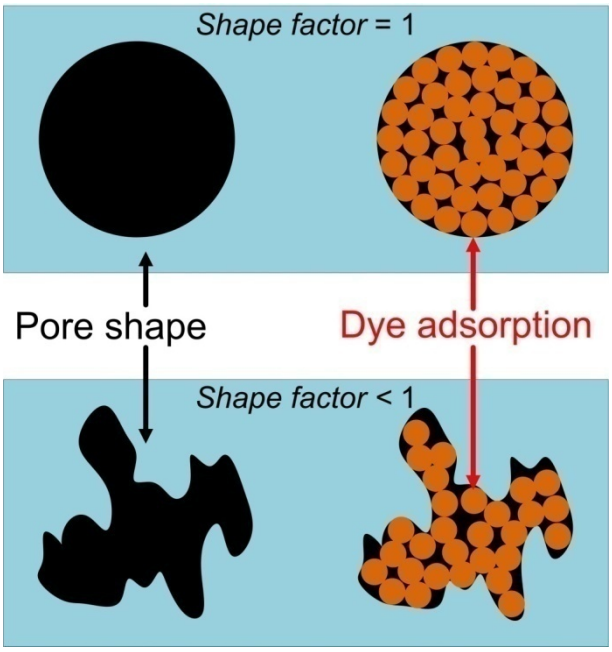

Figure 4.10 Graphics of dye adsorption in different pore shape. Reproduced with permission from ref [78]. Copyright (2016) Elsevier.

4.5 Reflectance

Figure 4.11 shows surface reflectance of texturing films. The lowest reflectance is clearly found for the texturing time of 4 min. A low reflectance refers an increment of light scattering in the internal film structure which can improve electron generation process and finally enhanced PCE as described in previous chapter [28]. In addition, the higher electron generation can be observed in the term of increased J_{sc}.

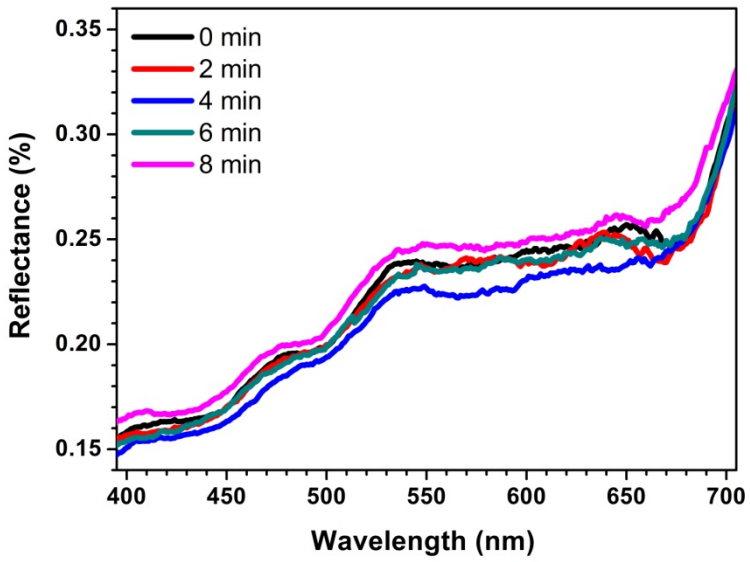

Figure 4.11 Reflectance of acid vapor texturing films. Reproduced with permission from ref [78]. Copyright (2016) Elsevier.

4.6 Raman shift

Raman shift of the non-texturing and texturing films at texturing time of 4 min was measured and shown in figure 4.12. Both of the films exhibit a similar of very low intensity peaks at 332 cm^{-1} and 383 cm^{-1} correspond to the multiphonon E_{2H}–E_{2L} mode and the A_{1T} mode, respectively. The strong intensity peak at 437 cm^{-1} corresponds to the optical phonon E_2 mode, which is the characteristic of the wurtzite hexagonal ZnO phase. The E_{1L} mode which is related to defects is observed at 578 cm^{-1} indicating the surface changed due to the chemical vapor corrosion. However, the relative low intensity means an irrelevant change.

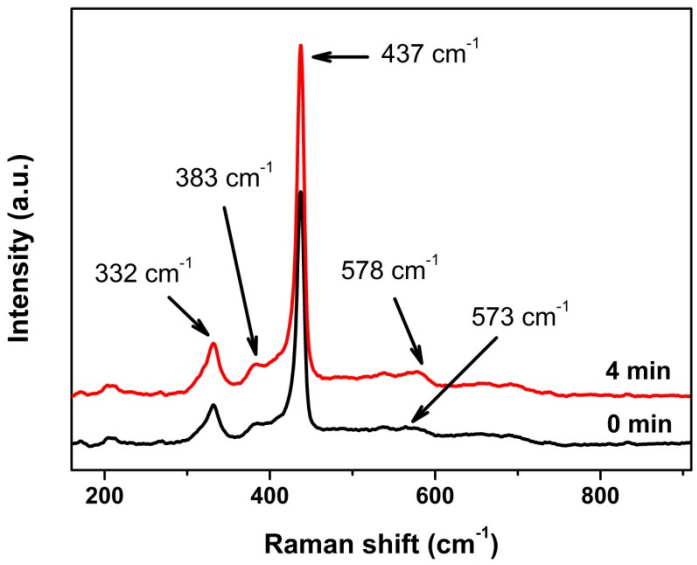

Figure 4.12 Raman shifts of the non-texturing and acid vapor texturing films. Reproduced with permission from ref [78]. Copyright (2016) Elsevier.

4.7 Dye adsorption

Figure 4.13 shows dye adsorption of N719 extracted from the photoelectrodes. The characteristic absorbance peak at the wavelength of 515 nm which represent to N719 is mentioned. In addition, amount of dye adsorption was calculated according to the Beer-Lambert law and listed in table 4.2. The dye adsorption is slightly increased for short texturing time. The maximum intensity is found at the texturing time of 4 min and it shows a 31.6% increased in comparison to the non-texturing film. Afterward, the intensity decreases in rapidly. It is noticed that the comparative increase in dye adsorption is directly related to the increase in pore density (39.3% increased up). From the result, it can be concluded that dye adsorption has a governing responsibility to pore density.

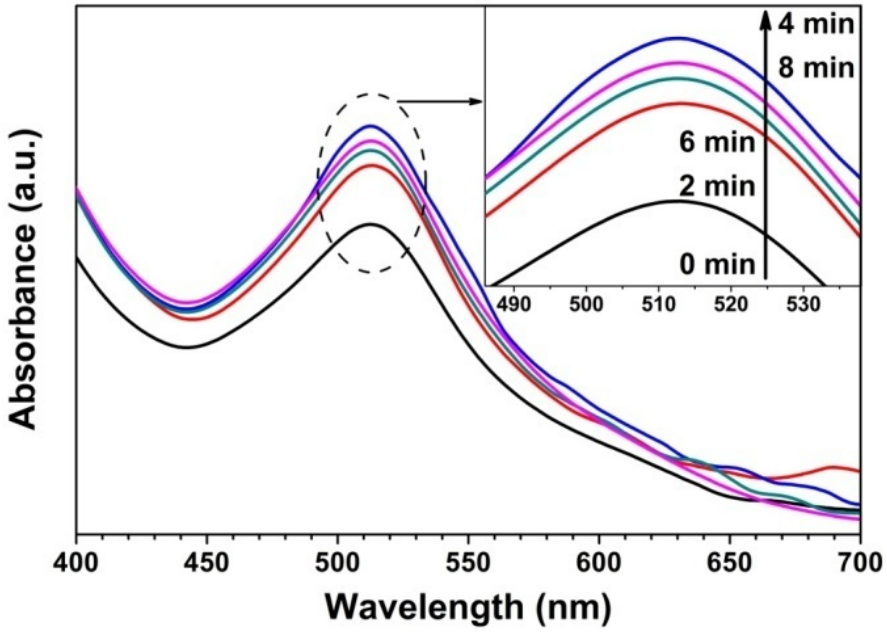

Figure 4.13 Absorbance of dye desorbed from acid vapor texturing films. Reproduced with permission from ref [78]. Copyright (2016) Elsevier.

Table 4.2 Dye adsorption of acid vapor texturing films. Reproduced with permission from ref [78]. Copyright (2016) Elsevier.

Texturing time (min)	Absorbance at 515 nm (a.u.)	Dye adsorption (10^{-9} moles/cm^2)
0	0.0587	49.6
2	0.0698	59.0
4	0.0772	65.3
6	0.0727	61.5
8	0.0744	63.0

4.8 Photovoltaic characteristics

DSSC devices fabricated with acid vapor texturing films were measured the J-V characteristics and shown in Figure 4.14 to evaluate the cell performance, and photovoltaic parameters are summarized in table 4.3. The device based on the 4 min texturing film shows the maximum PCE due to the increase in J_{sc}, the increased J_{sc} might be due to better dye adsorption which is in agreement with the pore density. While, small change in V_{oc} is observed. For FF, it slightly increases as decreasing thickness as can be seen in figure 4.15. The improvement of FF might be due to a better penetration of electrolyte in a thin layer and in a porous structure.

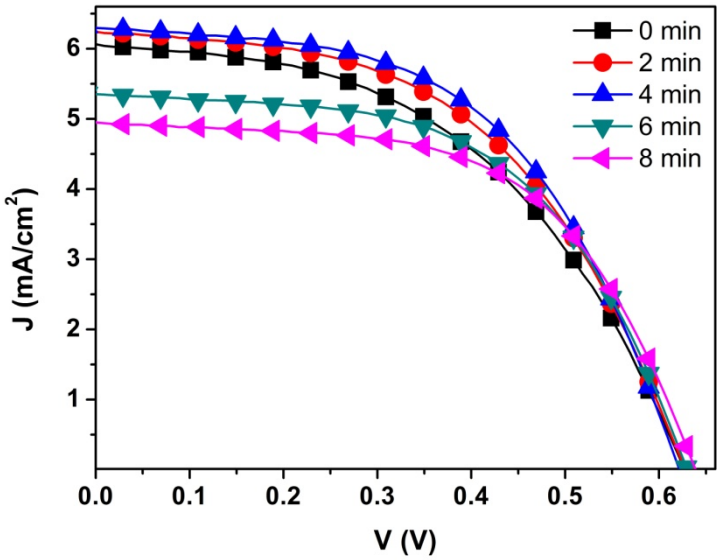

Figure 4.14 J-V characteristics of DSSCs fabricated with acid vapor texturing films. Reproduced with permission from ref [78]. Copyright (2016) Elsevier.

Table 4.3 Photovoltaic characteristics of DSSCs fabricated with acid vapor texturing films. Reproduced with permission from ref [78]. Copyright (2016) Elsevier.

Texturing time (min)	J_{sc} (mA/cm^2)	V_{oc} (V)	FF	PCE (%)
0	6.06 ± 0.07	0.62 ± 0.01	0.48 ± 0.01	1.83 ± 0.03
2	6.24 ± 0.06	0.62 ± 0.01	0.51 ± 0.02	1.99 ± 0.10
4	6.30 ± 0.09	0.62 ± 0.01	0.54 ± 0.02	2.08 ± 0.06
6	5.35 ± 0.03	0.62 ± 0.01	0.56 ± 0.01	1.88 ± 0.04
8	5.01 ± 0.13	0.63 ± 0.01	0.58 ± 0.02	1.83 ± 0.02

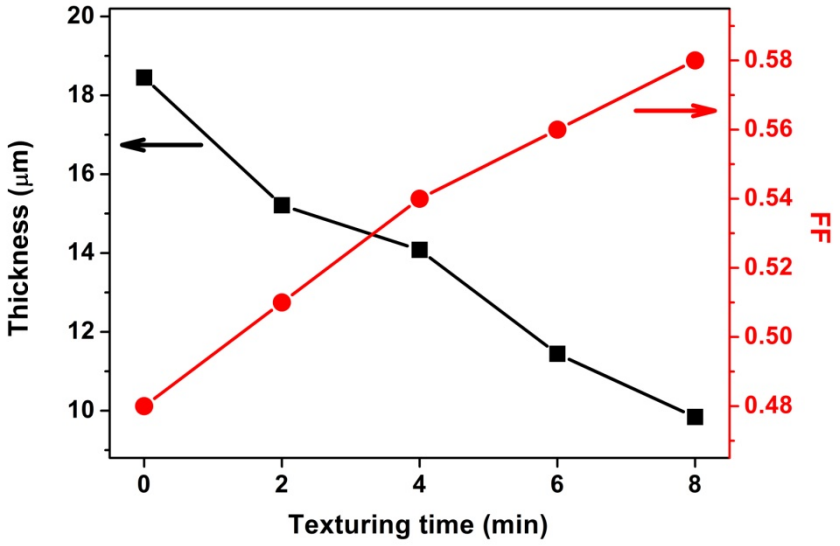

Figure 4.15 Plots of thickness and FF.

4.9 Investigation of influential factors on power conversion efficiency

To understand the effect of pore density on photovoltaic performance, the pore density, J_{sc} and PCE are plotted and shown in figure 4.16. It is clearly observed that J_{sc} and PCE changed in the relating trend of pore density. This result suggests that the pore density is a key factor to improve J_{sc} and finally enhance PCE. It is because a numerous pore density has ability to support more dye adsorption on texturing films which leading a higher dye adsorption and resulting a higher J_{sc}.

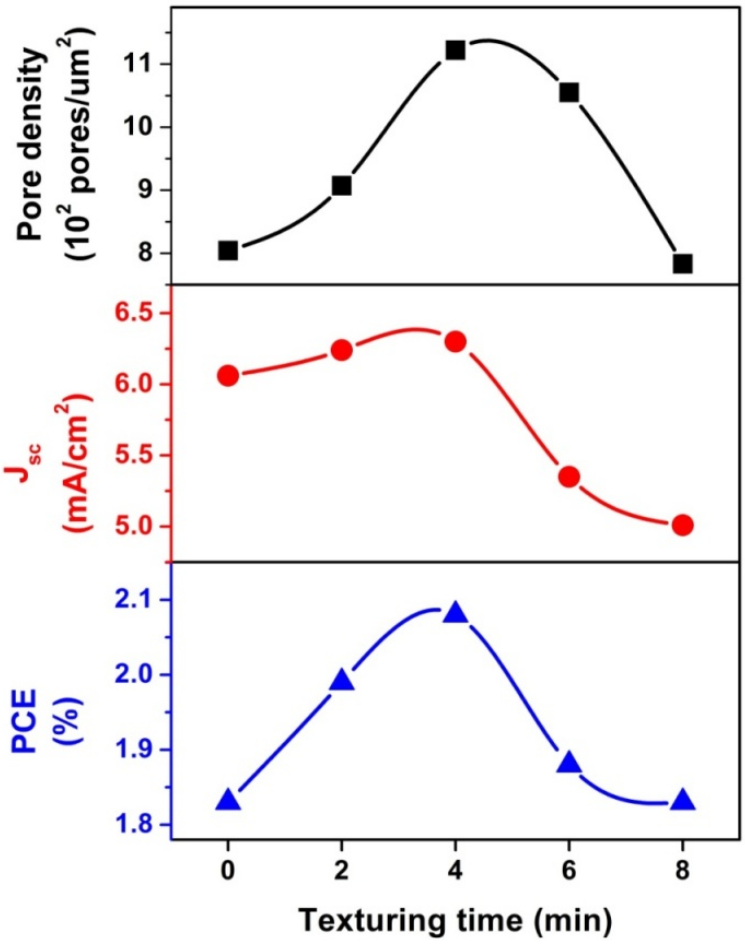

Figure 4.16 Graphics of dye adsorption in different pore shape. Reproduced with permission from ref [78]. Copyright (2016) Elsevier.

4.10 Electrochemical impedance spectroscopy analysis

A measurement of electrochemical impedance of these devices was performed under dark condition and forward bias of -0.7 V. Nyquist plots present a small increase in R_{rec} for texturing films based DSSCs which can be seen a larger semi-circle in comparison to the non-texturing films based DSSCs (figure 4.17). However, it is an insignificant achievement as can be seen a small different value in table 4.4 compare to the non-texturing films based DSSCs. The result implied that recombination behavior is not change after the texturing process. It can be assumed that the vapor texturing process has no relation to internal electrical property. Thus, the result confirms that dye adsorption is the influence factor for the vapor texturing process [81].

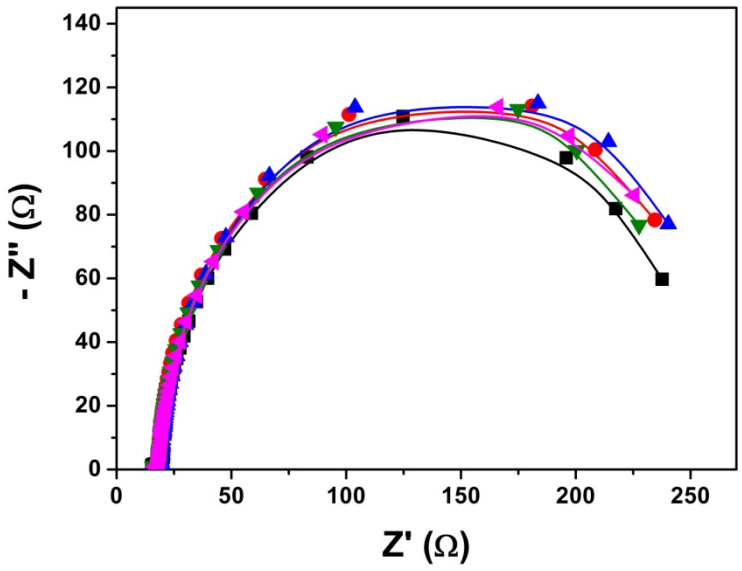

Figure 4.17 Nyquist plots of DSSCs fabricated with acid vapor texturing films. Reproduced with permission from ref [78]. Copyright (2016) Elsevier.

Table 4.4: EIS parameters of DSSCs fabricated with acid vapor texturing films.

Texturing time (min)	R_s (Ω)	R_{ct1} (Ω)	R_{ct2} (Ω)
0	14.70	4.88	226.30
2	14.98	3.11	244.40
4	17.21	2.46	241.00
6	16.04	2.51	234.40
8	15.84	3.39	240.40

4.11 Essential factors on short-circuit current density

From section 4.9, J_{sc} plays the important photovoltaic factor for enhancing DSSCs performance. It is well known that J_{sc} is influenced with dye adsorption and R_{rec}. To improved J_{sc}, higher dye adsorption and R_{rec} are required for increasing electron source and reducing recombination process, respectively. Thus, those factors are investigated and it is found that J_{sc}, dye adsorption and R_{rec} are changed in similar trends as shown in figure 4.18. The result confirms that both of increased dye adsorption and R_{rec} (reduced recombination) improve the DSSCs performance in this work.

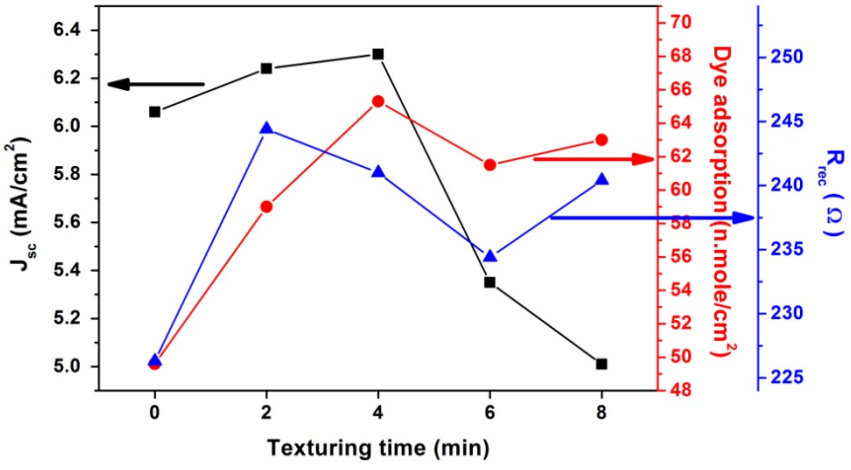

Figure 4.18 Plot of J_{sc}, dye adsorption and R_{rec}.

4.12 Summary of chemical vapor texturing process

A vapor texturing process using initial HNO_3 solution has an ability to create small porous ZnO films. Film properties included morphology, thickness, roughness, pore density and reflectance are investigated and its change after the texturing process. The pore density plays a significant parameter that involve to amount of dye adsorption. It is increased with a dominate correlation to the pore density. The increment of dye adsorption leads an improvement of short-circuit current density which is resulted an enhancement of power conversion efficiency. In addition, the increased short-circuit current density is also related to reduced electron recombination. This work demonstrates that an acid vapor texturing process using HNO_3 has an ability to modify porous ZnO films for improving dye adsorption, increasing light scattering and reducing electron recombination which is provided an enhanced power conversion efficiency of dye-sensitized solar cells.